Research Report

98-51

Mathematics and Computers in Simulation

T. Matsuo, S. Bernet, R.S. Colby*, T.A. Lipo

Wisconsin Power Electronic
Research Center
University of Wisconsin-Madison
Madison WI 53706-1691

*Otis Elevator Company
Five Farm Springs
Farmington, CT 06032

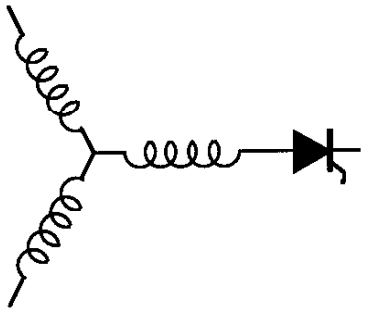

Wisconsin
Electric
Machines &
Power
Electronics
Consortium

University of Wisconsin-Madison
College of Engineering
Wisconsin Power Electronics Research Center
2559D Engineering Hall
1415 Engineering Drive
Madison WI 53706-1691

MATHEMATICS AND COMPUTERS IN SIMULATION

Mathematics and Computers in Simulation 46 (1998) 175–195

Modeling and simulation of matrix converter/induction motor drive

Takayoshi Matsuo[a,*], Steffen Bernet[a], R. Stephen Colby[b], Thomas A. Lipo[a]

[a] *University of Wisconsin-Madison, Electrical and Computer Engineering, 1415 Johnson Drive, Madison, Wisconsin 53706, USA*

[b] *Otis Elevator Company, Five Farm Springs, Farmington, Connecticut 06032, USA*

ELSEVIER

Publication Information

Mathematics and Computers in Simulation (ISSN 0378-4754). For 1998 Volumes 46–48 are scheduled for publication. A combined subscription to Mathematics and Computers in Simulation and Applied Numerical Mathematics (Volumes 26–28) at reduced rate is available.

Subscription prices are available upon request from the publisher. Subscriptions are accepted on a prepaid basis only and are entered on a calendar year basis. Issues are sent by surface mail except to the following countries where air delivery via SAL is ensured: Argentina, Australia, Brazil, Canada, China, Hong Kong, India, Israel, Japan, Malaysia, Mexico, New Zealand, Pakistan, Singapore, South Africa, South Korea, Taiwan, Thailand, United States. For all other countries airmail rates are available upon request.

Claims for missing issues must be made within six months of our publication (mailing) date.

For orders, claims, product enquiries (no manuscript enquiries) please contact the Customer Support Department at the Regional Sales Office nearest to you:

New York, Elsevier Science, P.O. Box 945, New York, NY 10159-0945, USA. Tel: (+1) 212-633-3730, [Toll Free number for North American Customers: 1-888-4ES-INFO (437-4636)], Fax: (+1) 212-633-3680, E-mail: usinfo-f@elsevier.com

Amsterdam, Elsevier Science, P.O. Box 211, 1000 AE Amsterdam, The Netherlands. Tel: (+31) 20-485-3757, Fax: (+31) 20-485-3432, E-mail: nlinfo-f@elsevier.nl

Tokyo, Elsevier Science 9-15, Higashi-Azabu 1-chome, Minato-ku, Tokyo 106-0044, Japan. Tel: (+81) 3-5561-5033, Fax: (+81) 3-5561-5047, E-mail: info@elsevier.co.jp

Singapore, Elsevier Science, No. 1 Temasek Avenue, #17-01 Millenia Tower, Singapore 039192. Tel: (+65) 434-3727, Fax: (+65) 337-2230, E-mail: asiainfo@elsevier.com.sg

Published monthly 0378-4754/98/$19.00 Printed in the Netherlands

ELSEVIER

Mathematics and Computers in Simulation 46 (1998) 175–195

MATHEMATICS AND COMPUTERS IN SIMULATION

Modeling and simulation of matrix converter/induction motor drive

Takayoshi Matsuo[a,*], Steffen Bernet[a], R. Stephen Colby[b], Thomas A. Lipo[a]

[a] *University of Wisconsin-Madison, Electrical and Computer Engineering, 1415 Johnson Drive, Madison, Wisconsin 53706, USA*

[b] *Otis Elevator Company, Five Farm Springs, Farmington, Connecticut 06032, USA*

Abstract

Modeling and simulation of a matrix converter/induction motor drive are presented in this paper, which includes a three phase ac to ac matrix converter, an induction motor, a field oriented controller, filters and a power source. In addition, a developed precise loss calculation model for power converters is described with calculation results when it was applied to the matrix converter. A harmonic analysis is described with a developed switching strategy, which reduces the harmonic current at the matrix converter input. © 1998 IMACS/Elsevier Science B.V.

1. Introduction

The ac to ac matrix converter was first investigated by Gyugyi and Pelly in 1976 [1]. More recently Venturini and Alesina have introduced a matrix converter design using a generalized high frequency switching strategy [2]. The matrix converter has recently attracted numerous researchers because of its simple topology, absence of large dc link capacitor, and easy control of input power factor. The purpose of this paper is to investigate via simulation the technical issues of applying the matrix converter to field oriented induction motor drives. In addition to the implementation of the drive system, a precise loss calculation model for power converters is described and applied to the drive system to study the loss characteristics of the matrix converter. The harmonic analysis of the matrix converter input current, the filter current, and the input power source current were performed to study the filter size and to develop a switching sequence combination which minimizes the harmonic contents of the matrix converter input current.

The simulation language ACSL [3] (Advanced Continuous Simulation Language) was used for this study, which is designed for modeling and evaluating the performance of continuous system described by time dependent, nonlinear differential equations and/or transfer functions. The language consists of a set of arithmetic operators, standard functions, a set of special ACSL statements, and a Macro capability.

* Corresponding author. Fax.: +1-4145128582; e-mail: tmatsuo@ra.rockwell.com

PII S0378-4754(97)00134-1

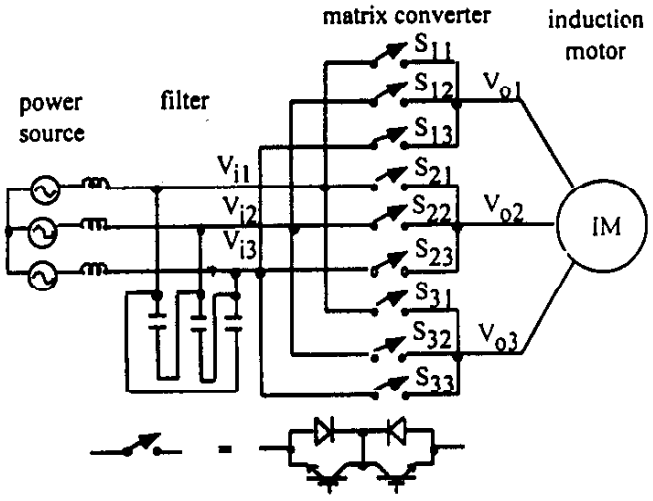

Fig. 1. Three phase ac to ac matrix converter.

2. Matrix converter/induction motor drive

A three phase ac to ac matrix converter basically consists of a 3 × 3 switch matrix. The 9 bi-directional voltage blocking, current conducting switches are arranged so that any input phase can be connected to any output phase at any time. The 3 × 3 switch matrix can be arranged in the form of Fig. 1 for purpose of analysis. Since an inductive load is assumed, the voltage sources of the input must be created by placing capacitors (filter) from line to line across the converter input phases. In principle, for a given set of input three phase voltages, any desired set of output voltages can then be synthesized by suitably toggling the matrix switches.

Fig. 2 shows a drive configuration for a field oriented control of an induction motor which is driven by a three phase to three phase matrix converter. By means of an incremental encoder or resolver, the angular position of the rotor θ_r is established. The angular position of the slip θ_s, which is calculated in the field oriented control module, is added to the angular position of the rotor θ_r to form the angular position of the stator MMF θ_e. These sinusoidal components are used to refer those physical stator currents from the physical (stationary) reference frame to the synchronously rotating (d–q) axes. The encoder is also used to measure speed. The voltage command signals from the field oriented controller are fed into the matrix converter block, where the matrix converter generates three phase PWM voltage pulses to drive the induction motor.

3. Three phase AC/AC matrix converter

Assuming that the voltages of the input are essentially constant during the switching interval, the average output voltage can be found during any switching interval by the equations

$$\frac{1}{T_s}\begin{bmatrix} V_{i1} & V_{i2} & V_{i3} \\ V_{i2} & V_{i3} & V_{i1} \\ V_{i3} & V_{i1} & V_{i2} \end{bmatrix}\begin{bmatrix} t_{1s} \\ t_{2s} \\ t_{3s} \end{bmatrix} = \begin{bmatrix} V_{o1} \\ V_{o2} \\ V_{o3} \end{bmatrix} \tag{1}$$

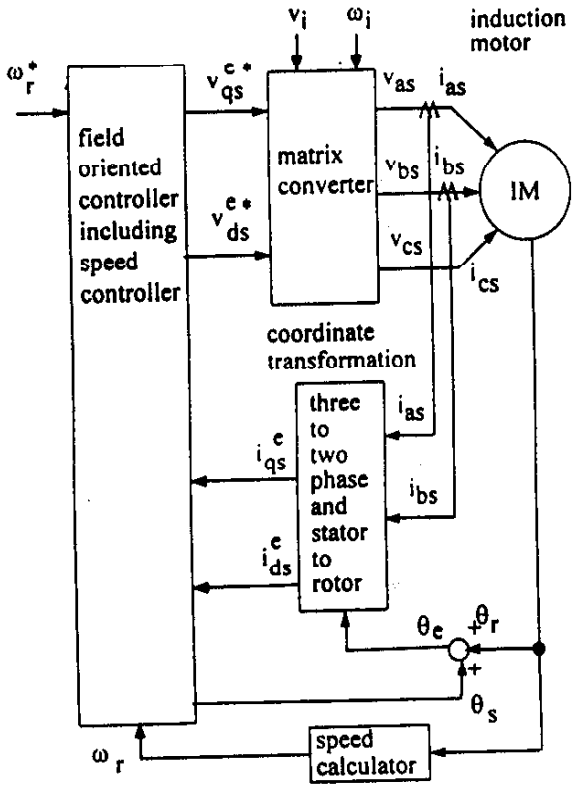

Fig. 2. Matrix converter/induction motor drive.

where

$$V_{iN} = V_I\cos(\omega_i t - (N-1)2\pi/3) \tag{2}$$

$$V_{oN} = V_O\cos(\omega_o t + \theta_o - (N-1)2\pi/3) \tag{3}$$

$$t_{1s} + t_{2s} + t_{3s} = T_s \tag{4}$$

$N = 1$, 2, and 3

where θ_o = arbitrary output voltage phase angle and T_s denotes the switching interval in seconds.

The three output voltages can also be synthesized by switching in the reverse direction such that during interval t_{1a}, phase a of the input is connected to phase a of the output, phase b of the input to phase c of the output and phase c of the input to phase b of the output. In effect the same output voltages can be generated except that the switches can be described by:

$$\frac{1}{T_s}\begin{bmatrix} V_{i1} & V_{i2} & V_{i3} \\ V_{i3} & V_{i1} & V_{i2} \\ V_{i2} & V_{i3} & V_{i1} \end{bmatrix}\begin{bmatrix} t_{1a} \\ t_{2a} \\ t_{3a} \end{bmatrix} = \begin{bmatrix} V_{o1} \\ V_{o2} \\ V_{o3} \end{bmatrix} \tag{5}$$

where

$$t_{1a} + t_{2a} + t_{3a} = T_s \tag{6}$$

Since the two switching strategies can produce exactly the same output voltage, in general, the output voltages can be formed by any combination of the symmetric Eq. (1) and antisymmetric Eq. (5) modes. That is,

$$\alpha_1 \frac{1}{T_s}\begin{bmatrix} V_{i1} & V_{i2} & V_{i3} \\ V_{i2} & V_{i3} & V_{i1} \\ V_{i3} & V_{i1} & V_{i2} \end{bmatrix}\begin{bmatrix} t_{1s} \\ t_{2s} \\ t_{3s} \end{bmatrix} + \alpha_2 \frac{1}{T_s}\begin{bmatrix} V_{i1} & V_{i2} & V_{i3} \\ V_{i3} & V_{i1} & V_{i2} \\ V_{i2} & V_{i3} & V_{i1} \end{bmatrix}\begin{bmatrix} t_{1a} \\ t_{2a} \\ t_{3a} \end{bmatrix} = \begin{bmatrix} V_{o1} \\ V_{o2} \\ V_{o3} \end{bmatrix} \tag{7}$$

where

$$\alpha_1 + \alpha_2 = 1 \tag{8}$$

It can be shown that while the output power factor angle ϕ_o is fixed by the load, the input power factor can be adjusted to any value consistent with Eqs. (9) and (10).

$$\alpha_1 = \frac{1}{2} + \frac{1}{2}\tan\phi_i \mathrm{ctn}\phi_o \tag{9}$$

$$\alpha_2 = 1 - \alpha_1 = \frac{1}{2} - \frac{1}{2}\tan(\phi_i)\mathrm{ctn}(\phi_o) \tag{10}$$

That is, if the power factor angle ϕ_o is given, then any value of ϕ_i can be chosen such that neither α_1 and α_2 are negative nor greater than one. That is, from inspection

$$-\phi_o \leq \phi_i \leq \phi_o \tag{11}$$

This equation demonstrates that the input power factor can always be made unity. In fact if the power factor is, for example, 60 degrees lagging, the input power factor can be adjusted to be as much as 60 degrees leading.

It should be noted that regardless of the switching strategy adopted, there are, however, physical limits on the output voltage achievable with this system. For complete control of the output voltage at any time, the envelope of the target output voltages must be wholly contained within the continuous envelope of the input voltages. This limit can be improved by adding a third harmonic at the input frequency to all target voltages [4]. The addition of this third harmonic increases the available output voltage range to 0.75 of the input when the third harmonic has a peak value of $V_I/4$. Further improvement of the transfer ratio can be achieved by subtracting a third harmonic at the output frequency from all target output voltages to minimize the range of the output voltage envelope to 0.866 of the peak phase voltage which allows an absolute maximum transfer ratio of 0.75/0.866=0.866 of V_I when this third harmonic has a peak value of $V_O/6$. Hence the maximum possible voltage transfer ratio becomes V_O/V_I=0.75/0.866=0.866. A modulation strategy [$M(t)$] can be found such that [4]

$$[M(t)].[V_I(t)] = V\begin{bmatrix} \cos(\omega_o t + \theta_o) \\ \cos(\omega_o t + \theta_o - \frac{2\pi}{3}) \\ \cos(\omega_o t + \theta_o + \frac{2\pi}{3}) \end{bmatrix} + \frac{V_O}{2\sqrt{3}}\begin{bmatrix} \cos(3\omega_i t) \\ \cos(3\omega_i t) \\ \cos(3\omega_i t) \end{bmatrix} - \frac{V_O}{6}\begin{bmatrix} \cos(3\omega_o t + 3\theta_o) \\ \cos(3\omega_o t + 3\theta_o) \\ \cos(3\omega_o t + 3\theta_o) \end{bmatrix} = [V_O] \tag{12}$$

The switching periods $t_{ij}(t)$ are given by the equation

$$[T_{sw}(t)] = \begin{bmatrix} t_{11}(t) & t_{12}(t) & t_{13}(t) \\ t_{21}(t) & t_{22}(t) & t_{23}(t) \\ t_{31}(t) & t_{32}(t) & t_{33}(t) \end{bmatrix} = T_s[M(t)] \tag{13}$$

One can refer to [4] for the equations for $[M(t)]$.

4. Matrix converter model

The implementation of the equations to calculate the switching periods $t_{ij}(t)$ for 9 bi-directional switches with the simulation language ACSL is straight forward because ACSL is a FORTRAN based language. The bi-directional switches are treated as ideal switches in the simulation program. The conditional switch function RSW, which is available in ACSL, was used to obtain voltage pulses which are associated with each switching interval. For example, to calculate the phase 1 output voltage, the corresponding ACSL instructions are

$$\text{vo11} = \text{RSW}((\text{ta.GT.0.0.AND.ta.LE.t11}), \text{vi1}, 0.0) \tag{14}$$

$$\text{vo12} = \text{RSW}((\text{tb.GT.0.0.AND.tb.LE.t12}), \text{vi2}, 0.0) \tag{15}$$

$$\text{vo13} = \text{RSW}((\text{tc.GT.0.0.AND.tc.LE.t13}), \text{vi3}, 0.0) \tag{16}$$

The phase 1 output voltage is expressed as

$$\text{vo1} = \text{vo11} + \text{vo12} + \text{vo13} \tag{17}$$

where tb=ta−t11 and tc=tb−t12. The instruction line of Eq. (14) means that the phase 1 output is connected to the phase 1 input for the time period from ta=0 to ta=t11, that is, vo11=vi1 if 0.0< ta < t11, otherwise vo11=0.0. The time ta is reset to zero at the beginning of each switching period Ts. The phase 2 and 3 output voltages can be calculated in the same manner.

$$\text{vo21} = \text{RSW}((\text{ta.GT.0.0.AND.ta.LE.t21}), \text{vi1}, 0.0) \tag{18}$$

$$\text{vo22} = \text{RSW}(\text{tc.GT.0.0.AND.tc.LE.t22}), \text{vi2}, 0.0) \tag{19}$$

$$\text{vo23} = \text{RSW}(\text{td.GT.0.0.AND.td.LE.t23}), \text{vi3}, 0.0) \tag{20}$$

$$\text{vo21} = \text{RSW}((\text{ta.GT.0.0.AND.ta.LE.t31}), \text{vi1}, 0.0) \tag{21}$$

$$\text{vo22} = \text{RSW}(\text{te.GT.0.0.AND.te.LE.t32}), \text{vi2}, 0.0) \tag{22}$$

$$\text{vo23} = \text{RSW}(\text{tf.GT.0.0.AND.tf.LE.t33}), \text{vi3}, 0.0) \tag{23}$$

The phase 2 and 3 output voltages are expressed as

$$\text{vo2} = \text{vo21} + \text{vo22} + \text{vo23} \tag{24}$$

$$\text{vo3} = \text{vo31} + \text{vo32} + \text{vo33} \tag{25}$$

where tc=ta−t21, td=tb−t22, te=ta−t31, and tf=tc−t22.

Similar instructions are used to calculate input currents.

$$\text{ii11} = \text{RSW}((\text{ta.GT.0.0.AND.ta.LE.t11}), \text{io1}, 0.0) \tag{26}$$

$$\text{ii21} = \text{RSW}((\text{tb.GT.0.0.AND.tb.LE.t12}), \text{io1}, 0.0) \tag{27}$$

$$\text{ii31} = \text{RSW}((\text{tc.GT.0.0.AND.tc.LE.t13}), \text{io1}, 0.0) \tag{28}$$

$$\text{ii12} = \text{RSW}((\text{ta.GT.0.0.AND.ta.LE.t21}), \text{io2}, 0.0) \tag{29}$$

$$\text{ii22} = \text{RSW}((\text{tc.GT.0.0.AND.tc.LE.t22}), \text{io2}, 0.0) \tag{30}$$

$$\text{ii32} = \text{RSW}((\text{td.GT.0.0.AND.td.LE.t23}), \text{io2}, 0.0) \tag{31}$$

$$\text{ii13} = \text{RSW}((\text{ta.GT.0.0.AND.ta.LE.t31}), \text{io3}, 0.0) \tag{32}$$

$$\text{ii23} = \text{RSW}((\text{te.GT.0.0.AND.te.LE.t32}), \text{io3}, 0.0) \tag{33}$$

$$\text{ii33} = \text{RSW}((\text{tf.GT.0.0.AND.tf.LE.t33}), \text{io3}, 0.0) \tag{34}$$

The phase 1, 2 and 3 input currents are expressed as

$$\text{ii1} = \text{ii11} + \text{ii12} + \text{ii13} \tag{35}$$

$$\text{ii2} = \text{ii21} + \text{ii22} + \text{ii23} \tag{36}$$

$$\text{ii3} = \text{ii31} + \text{ii32} + \text{ii33} \tag{37}$$

5. Induction motor model

The simulation equations for an induction motor in the d–q stationary reference frame are typically described, for the q-axis stator winding, as [5]

$$\lambda_{qs} = \int \left(v_{qs} + \frac{r_s}{l_{ls}} (\lambda_{mq} - \lambda_{qs}) \right) dt \tag{38}$$

$$\lambda_{mq} = \frac{L_m^*}{l_{ls}} \lambda_{qs} + \frac{L_m^*}{l_{lr}} \lambda_{qr} \tag{39}$$

$$i_{qs} = \frac{\lambda_{qs} - \lambda_{mq}}{l_{ls}} \tag{40}$$

$$T_e = \frac{3}{2}\frac{P}{2} (\lambda_{ds} i_{qs} - \lambda_{qs} i_{ds}) \tag{41}$$

where

$$L_m^* = 1 \Big/ \frac{1}{l_{ls}} + \frac{1}{l_{lr}} + \frac{1}{L_m} \tag{42}$$

and λ denotes flux linkage, v and i denote voltage and current, respectively. Quantities with subscript q or d denote q-axis or d-axis quantities and quantities with subscript s or r denote stator or rotor quantities. r_s and r_r are stator and rotor resistance and ω_r is rotor speed. l_{ls} and l_{lr} are stator and rotor

leakage inductances and L_m is the magnetizing inductance. T_e is the motor torque and P is the number of poles. Similar equations apply for the remaining d–q compoents [5].

The stator and rotor flux linkage equations are described in the form of integration, which is suitable for the simulation language ACSL. Eq. (38) is described as Eq. (43) in ACSL.

$$\text{lamdaqs} = \text{INTEG}(\text{vqs} - \text{rs}^*\text{iqs}, \text{lamdaqs0}) \tag{43}$$

It is important to use the line to line voltage to perform the three phase to d–q coordinate transformation because each phase voltage of the matrix converter contains the third harmonic components to improve the output to input voltage ratio. The coordinate transformation equations to relate the matrix converter model to the induction motor model are,

$$v_{qs} = \frac{V_{abs} - V_{cas}}{3} \tag{44}$$

$$v_{ds} = \frac{-V_{bcs}}{\sqrt{3}} \tag{45}$$

where $v_{abs}=v_{o1}-v_{o2}$, $v_{bcs}=v_{o2}-v_{o3}$, and $v_{cas}=v_{o3}-v_{o1}$.

6. Field oriented controller model

A field oriented controller based on d–q current controllers in synchronous reference frame is implemented. A typical d–q differential equation in synchronous reference frame is, [5]

$$v^e_{qs} = r_s i^e_{qs} + p\lambda^e_{qs} + \omega_e \lambda^e_{ds} \tag{46}$$

where

$$\lambda^e_{qs} = L_s i^e_{qs} + L_m i^e_{qr} \tag{47}$$

where quantities with the superscript e denote quantities in synchronous reference frame. The conditions of the field oriented control, which enable that the rotor flux vector has only one component λ^e_{dr} in the d-axis ($\lambda^e_{qr} = 0$), are described as

$$i^{e*}_{qs} = \frac{2}{3}\frac{2}{P}\frac{L_r}{L_m}\frac{T^*_e}{\lambda^{e*}_{dr}} \tag{48}$$

$$i^{e*}_{ds} = \frac{1}{L_m}\lambda^{e*}_{dr} + \frac{L_r}{L_m r_r} p\lambda^{e*}_{dr} \tag{49}$$

$$\omega^*_s = i^{e*}_{qs}\frac{r_r}{L_r}\frac{L_m}{\lambda^{e*}_{dr}} \tag{50}$$

Fig. 3 shows a block diagram of a field oriented control of an induction motor including a speed controller. The required slip angular frequency ω_s to produce a specific motor torque is calculated based on the d–q current commands and motor parameters, which is shown in Fig. 4, and is integrated to obtain the slip angular position θ_s. Current regulators guarantee that the desired and actual values of the

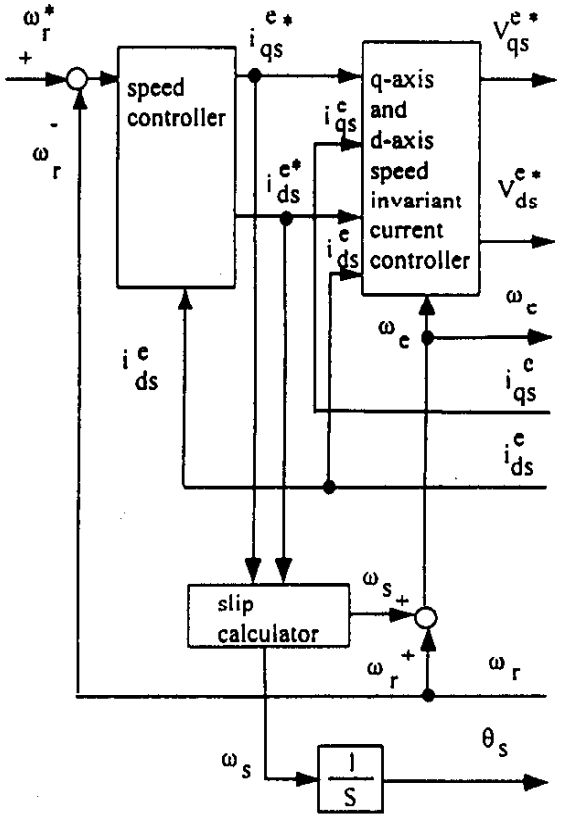

Fig. 3. A block diagram of a field oriented controller including a speed controller.

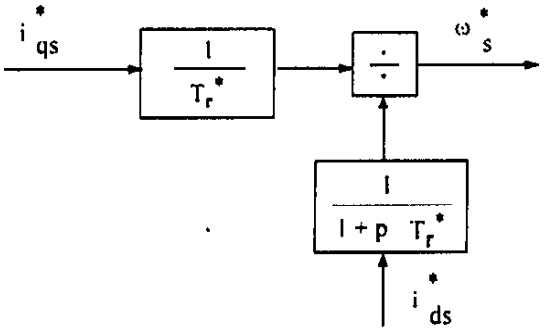

Fig. 4. Slip calculator.

d–q currents are obtained. The voltage command signals which are obtained in the synchronously rotating d–q frame are, with the stator MMF angular speed, fed into the matrix converter block to produce PWM switching pulses for the matrix converter.

The exact nature of the speed invariant current control block is explained in Fig. 5. Referring to the stator voltage equations for an induction machine, Eq. (46) for example, the presence of the "counter emf terms" $\omega_e\lambda^e_{ds}$ and $\omega_e\lambda^e_{qs}$ is recalled. When speed changes rapidly, these terms cause an error in the current regulator since the integrators of the two PI current controllers must continually integrate at a

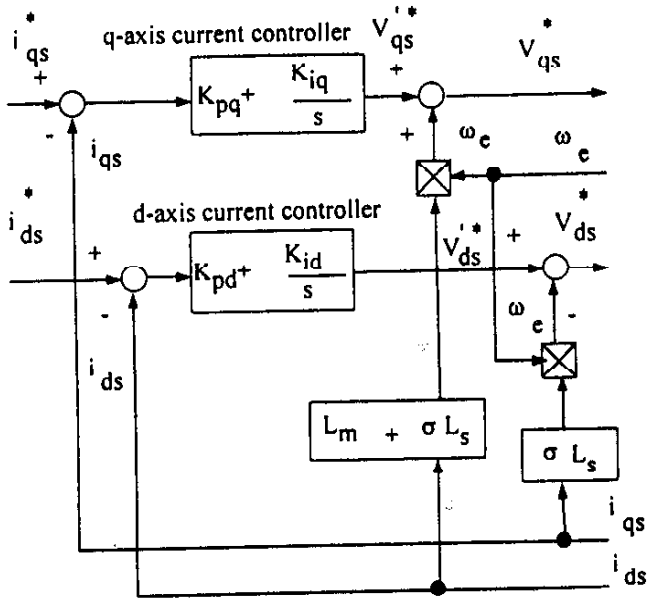

Fig. 5. Details of the speed invariant d–q current regulator.

rate proportional to speed due to the cemf terms in addition to performing their function of regulating the two components of stator current. This requirement can be eliminated by supplying the counter emf portion of the applied voltage separately by means of feed forward control as shown in Fig. 5. In this figure, the speed voltage components $\omega_e\lambda^e_{ds} = \omega_e L_m i^e_{ds} + \omega_e \sigma L_s i^e_{ds}$, and $\omega_e\lambda^e_{qs} = -\omega_e \sigma L_s i^e_{qs}$ are added to the outputs of the current regulators, v^*_{qs} and v^*_{qs} form the applied voltages in the d–q frame, v^*_{qs} and v^*_{qs}, where $\sigma L_s = 1 - L^2_m/L_s L_r$.

The implementation of the field oriented controller into an ACSL simulation program is straight forward. PI controllers can be implemented with ACSL operators such as LIMINT. An ACSL statement described by Eq. (51) performs an integration of iqer*iqki with an initial value of vq0, a bottom bound on vqint of −vqmax, and a top bound on vqint of vqmax.

$$\text{vqint} = \text{LIMINT}(\text{iqer*iqki}, \text{vq0}, -\text{vqmax}, \text{vqmax}) \tag{51}$$

7. Input filter and power source model

The three phase to three phase matrix converter is completed by filters at the input side. The output side filters can generally be omitted in motor drive applications, where the stator winding inductances of the motor work as the filters. One important role of the filters at input side is to keep the input voltage from changing significantly during each PWM cycle. Another important role is to absorb harmonic currents, which are generated by matrix converters, to prevent unwanted harmonic currents from flowing into ac main supplies and to satisfy any power quality regulation applicable.

A simple filter configuration was examined, as shown in Fig. 6, where a capacitor is connected between each line to line at the matrix converter input. The equations for one phase of the filter and

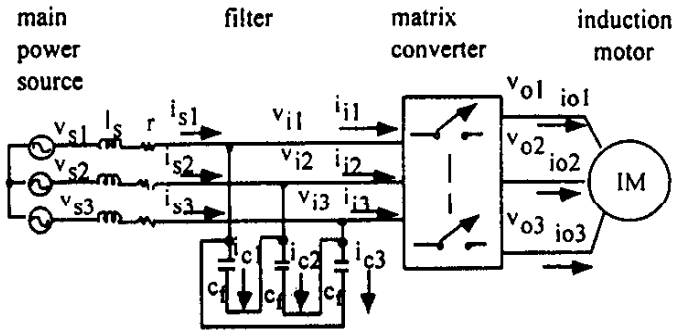

Fig. 6. Input filters and main power source of a matrix converter/induction motor drive.

power source are given as,

$$v_{s1} - v_{i1} = ri_{s1} + l_s \frac{di_{s1}}{dt} \tag{52}$$

$$i_{c1f} = i_{s1} - i_{i1} \tag{53}$$

$$i_{c1} = \frac{i_{c1f} - i_{c2f}}{3} \tag{54}$$

$$v_{c1} = \frac{1}{c_f} \int i_{c1} dt \tag{55}$$

$$v_{i1} = \frac{v_{c1} - v_{c3}}{3} \tag{56}$$

where l_s and r denote the leakage inductance and resistance of the power source and $v_{s1\sim3}$ are three phase source voltages. The remainder of the filter equations are apparent by symmetry.

8. Simulation results

To illustrate the use of these equations, a simulation was carried out with the input source line to line voltage of 480 V rms. The filter capacitance of 10 μF and the induction motor rating of 40 kW was used for this simulation run. A waveform of the phase a motor current and a filtered waveform of the phase a matrix converter output voltage are shown in Fig. 7. The matrix converter output voltage includes third harmonic components at both the input frequency and output frequency in addition to the fundamental component. Both third harmonic components do not appear on the line to line motor voltages because each matrix converter three phase output voltage has the same third harmonic component. Fig. 8 shows a waveform of the phase a matrix converter output voltage for 3 ms. The wave form of v_{o1} in Fig. 7 is a filtered waveform of v_{o1} in Fig. 8. Typical waveforms of the voltage across one bi-directional switch and the switch current are presented in Fig. 9. Fig. 10 shows how the capacitors at the matrix converter input work as the filters. Most of the harmonic components of the matrix converter input currents are absorbed into the filter capacitors. The voltage and current waveforms of the input main power source are shown in Fig. 11, where it is demonstrated that the input power factor is controlled at near unity value.

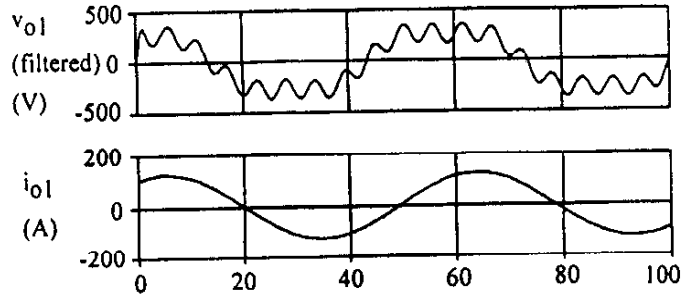

Fig. 7. A waveform of the phase a motor current and a filtered waveform of the phase a matrix converter output voltage showing added third harmonic components at both the input and output frequencies.

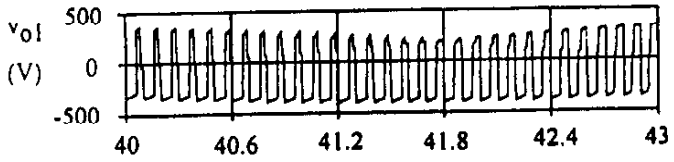

Fig. 8. A waveform of the phase a matrix converter output voltage.

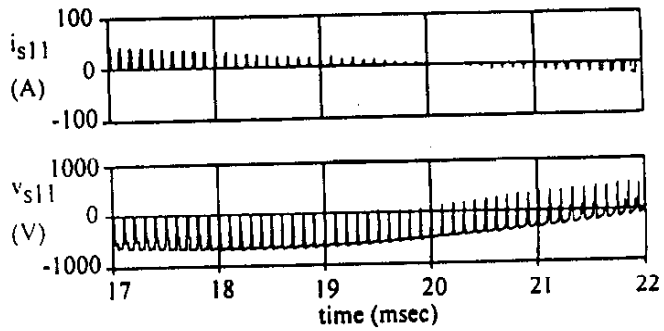

Fig. 9. Waveforms of the switch voltage and current, which is connected between the input phase 1 and the output phase 1.

The switching frequency of the matrix converter was set at 10 kHz, that is, the sampling interval of 100 μs. The integration cycle in the ACSL program was set to carry out every 1 μs.

9. Harmonic current analysis

Harmonic components of the matrix converter input currents, filter capacitor currents, and input source currents were analyzed to determine the size of the filter using the FFT (Fast Fourier Transformation) function in MATLAB. A numerical data file for each current/voltage is generated with ACSL program.

Then, MATLAB processes the data for FFT. The ACSL program generates data points of waveforms every 1 μs in the simulation described in Section 6. A FFT was performed for the data points of at least 1 cycle of output frequency, that is, when the output frequency is 10 Hz the data file has 100,000 points

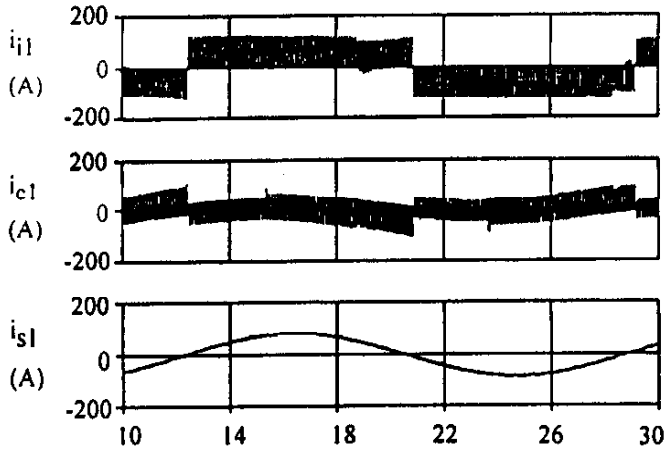

Fig. 10. Waveforms of the matrix converter input current, the filter capacitor current and the input current of the main power source.

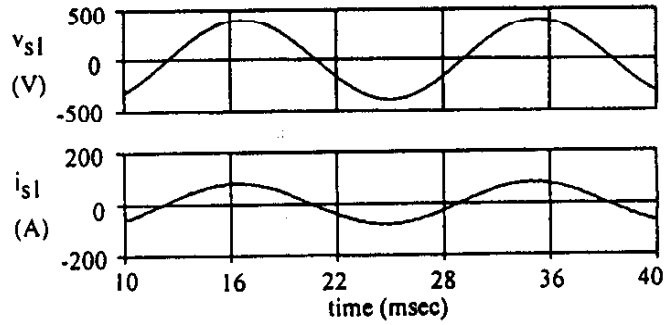

Fig. 11. Waveforms of the input voltage and current of the main power source.

for 100 ms of data. MATLAB also calculates rms value and distortion index for each waveform and creates plot files for spectrum profiles. Typical spectrum profiles of the matrix converter input current, the filter capacitor current and the input power source current are shown in Fig. 12.

10. Switching strategy

An Optimized pulse pattern to minimize the input current harmonics, presented in Ref. [3], was implemented in the simulator for its switching strategy. Each output phase of a three phase to three phase matrix converter is connected to each three input phase for a certain time period during each switching interval. Each time period is determined so that each output (Fig. 12) voltage is to be an average voltage of three input voltage pulses.

$$v_{o1} = v_{i1} * \frac{t_{11}}{T_s} + v_{i2} * \frac{t_{12}}{T_s} + v_{i3} * \frac{t_{13}}{T_s} \tag{57}$$

$$v_{o2} = v_{i1} * \frac{t_{21}}{T_s} + v_{i2} * \frac{t_{22}}{T_s} + v_{i3} * \frac{t_{23}}{T_s} \tag{58}$$

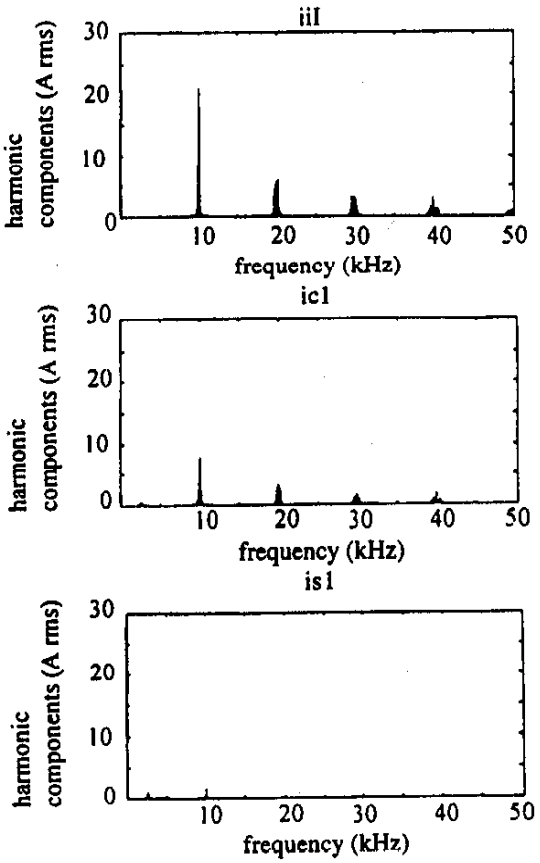

Fig. 12. Spectrum profiles of the matrix converter input current, the filter capacitor current, and the input source current.

$$v_{o3} = v_{i1} * \frac{t_{31}}{T_s} + v_{i2} * \frac{t_{32}}{T_s} + v_{i3} * \frac{t_{33}}{T_s} \tag{59}$$

The input phase 1 voltage appears in output phase 1 for a time interval t_{11}, the input phase 2 voltage for a time interval t_{12}, and the input phase 3 voltage for a time interval t_{13}, where $t_{11} + t_{12} + t_{13} = T_s$ and the switching interval $T_s = 1/f_s$ (f_s is the switching frequency). When the switching frequency f_s is 10 kHz the switching interval $T_s = 100\,\mu s$. There is no restriction on the sequence of the three time interval, that is, the output phase 1 can be connected to the input phase 2 first and then phase 3 and phase 1, or to the input phase 3 first and then phase 1 and phase 2. The output voltage v_{o1} remains same in either switching sequence combinations. There are basically 216 different switching sequence combinations for a nine-switch three phase to three phase matrix converter to produce specific three phase output voltages. Matrix converter input current characteristics depend on the switching sequence combinations while output current characteristics are not significantly affected by the change of the switching sequence combinations.

It was found [6] that the input current rms value can be reduced by applying proper switching sequence combinations, which increase the time period when all the three output phases are short circuited at the matrix converter input. The condition can be achieved by switching the three switches connected to the same input phase at the same time. The switching sequence combinations illustrated in

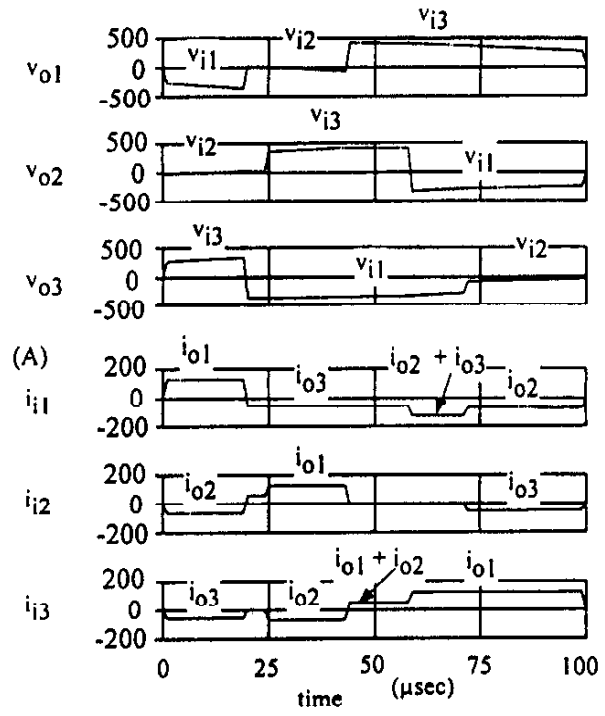

Fig. 13. Illustration of one of the switching sequence combinations showing waveforms of three phase output voltages and three phase input currents during one switching interval.

Figs. 13 and 14 produce the same fundamental components for both output voltages and input currents. However, the total rms values of the phase 1, 2 and 3 input currents of Fig. 14 are 17%, 39%, and 39% less than the ones of Fig. 13, respectively. There exist two other switching sequence combinations that produce minimum total rms values of the input currents, which are the alternative schemes to the one illustrated in Fig. 14. Balanced three phase input current can be obtained by alternating the three switching sequence combinations. Low alternating frequency keeps the lowest major harmonic components near the switching frequency.

11. Semiconductor loss model

The implementation of physical semiconductor models is often not possible or very inefficient in large systems to be simulated. This is especially the case in the drive system depicted in Fig. 1 where each of the nine forward and reverse blocking bi-directional current conducting switches is realized by a back to back arrangement of IGBTs (Common Collector Configuration [6]). Since each four-quadrant switch (4QSW) consists of 2 IGBTs and 2 diodes, the semiconductor losses of 18 IGBTs and 18 diodes have to be detected. To solve this problem at low computation time a semiconductor loss model has been developed which allows on the basis of ideal switching transients a sufficiently accurate loss estimation of each semiconductor. The loss model contains besides an analytical description of the significant losses especially an algorithm which determines the type of each occurring switching transient and distributes the losses to the active semiconductors (2 IGBTs, 2 diodes) of the switches.

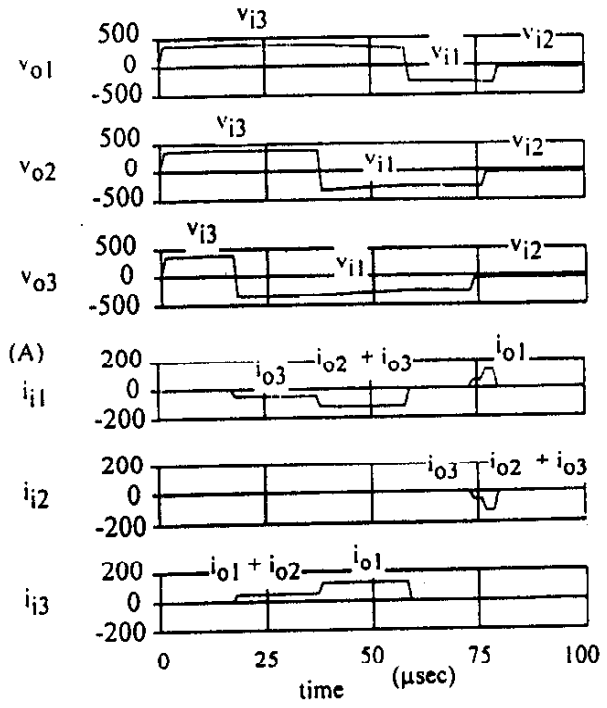

Fig. 14. Illustration of one of the switching sequence combinations, which reduces the harmonic components of the matrix converter input currents, showing waveforms of three phase output voltages and three phase input currents during one switching interval.

The commutation of an output phase current from one switch to another in each of the three switch groups can be described by the equivalent commutation circuit presented in [7]. Two fundamental commutations can be distinguished according to the instantaneous power of the load- the inductive commutation with a positive gradient of power and the capacitive commutation with a negative gradient of power.

The inductive commutation is initiated by a hard turn-on transient of a 4QSW (IGBT) and completed by the passive turn-off transient of the other 4QSW (diode) during the interruption of the reverse current. In contrast to this the capacitive commutation is characterized by a hard turn off transient (IGBT) and a low loss passive zero voltage turn on transient (diode). Detailed investigations of the switching losses of hard switching 4QSWs showed that nearly all switching losses are caused by the active turn on transient of the IGBTs (W_{ONT}) as well as the reverse recovery losses of the diodes (W_{OFFD}) during the inductive commutation and the active turn off transient of the IGBTs (W_{OFFT}) during the capacitive commutation.

The basis of the model is the analytical description of these switching losses and the on-state voltages at junction temperatures of T_j=25°C and T_j=125°C approximated by the following equations:

$$V_{CE} = (V_{0T} + R_{0T} \cdot i_S^{B_{conT}}) \cdot \left(1 - \frac{125°C - T_j[°C]}{100°C} C_{conT}\right) \tag{60}$$

$$V_D = (V_{0D} + r_{0D} \cdot i_S^{B_{conD}}) - (T_j[°C] - 125°C) \cdot C_{conD}) \tag{61}$$

$$W_{ONT} = (A_{ONT} \cdot i_S^{B_{ONT}}) \left(1 - \frac{125°C - T_j[°C]}{100°C} C_{ONT}\right) \cdot F \tag{62}$$

$$W_{OFFT} = (A_{OFFT} \cdot i_S^{B_{OFFT}}) \left(1 - \frac{125°C - T_j[°C]}{100°C} C_{OFFT}\right) \cdot F \tag{63}$$

$$W_{OFFD} = (A_{OFFD} \cdot i_S^{B_{OFFD}}) \left(1 - \frac{125°C - T_j[°C]}{100°C} C_{OFFD}\right) \cdot F \tag{64}$$

$$F = \left(1 - \frac{600V - |v_c[V]|}{600V}\right) \tag{65}$$

where

v_c	Commutation voltage
T_j	Junction temperature
v_o	Bias voltage at T_j=125°C
r_o	Dynamic resistance at T_j=125°C
A,B,C	Curve fitted constants at T_j=125°C, (v_c=600 V)

The fitting of the on-state voltages and switching losses for IGBT and diode of the considered 1200 V/300 A NPT-IGBT module SKM400GA122D with "Mathematica" has produced the constants given in Table 1. It should be mentioned that the correspondence between the data contained in the data sheet and the fitted functions is excellent for both the on-state voltages and the switching losses of IGBT and diode (relative error 5%).

Fig. 15 shows the flow chart of the implemented IGBT and diode loss model for the switch group sg1 (S_{11},S_{12},S_{13}) of the matrix converter. Because the program parts of the other two switch groups are completely dual it is sufficient to discuss only the represented flow chart.

First, the state of all switches of the matrix converter is fixed to a starting position in the "Initial" section of the simulation program. Starting with the run of the integration algorithm in the "Derivative" section the values of the input voltages and output currents of the matrix converter are computed for

Table 1
Fitted parameters of the NPT-IGBT module SKM400GA122D (1200 V/300 A) for loss calculation

	IGBT	Diode
$v_{0T/D}$	0.55	0.4
$r_{0T/D}$	0.11	0.11
$B_{conT/D}$	0.55	0.49
$C_{conT/D}$	0.16	0.00396
A_{ONT}	0.18	
B_{ONT}	1.01	
C_{ONT}	0.36	
$A_{OFFT/D}$	0.49	0.22
$B_{OFFT/D}$	0.79	0.65
$C_{OFFT/D}$	0.165	0.69

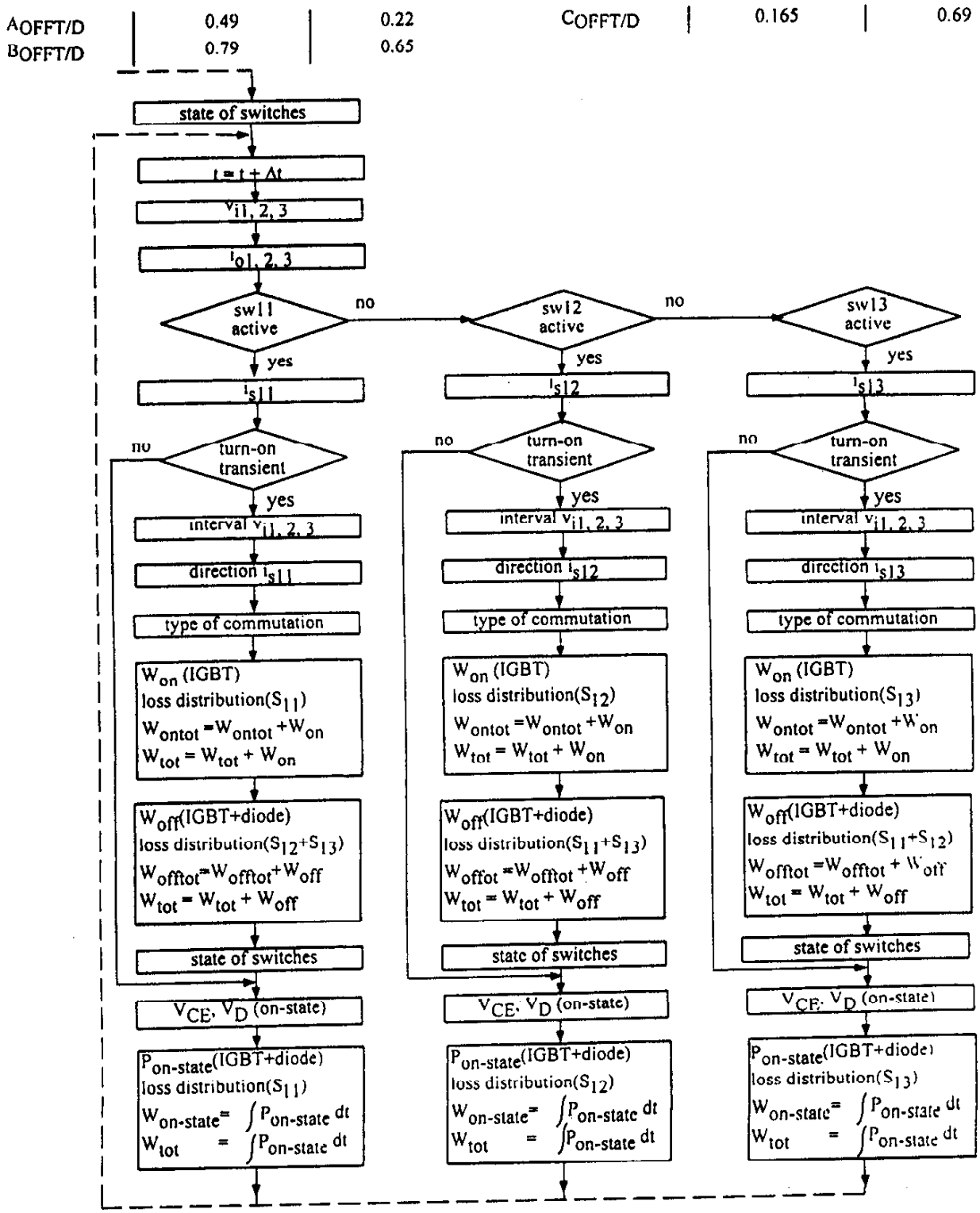

Fig. 15. Flow chart of the implemented semiconductor loss model for one switch group of the matrix converter.

each integration step Δt. The actual loss model begins with a renewed observation of the turned on switches and a determination of the switch currents on the basis of the current duty cycles. If the active switch was turned on with the new integration step initially, the type of the occurring commutation is determined by an analysis of the directions of the commutation voltage (voltage interval) and the load current [7]. Afterwards the turn on losses are computed corresponding to the current values of the switch current, the line to line voltage and the junction temperature. The distribution of the turn on losses to the semiconductors of a switch (which means the addition of the occurring turn on losses to the total turn on losses and the total semiconductor losses of the turning on device) is possible by an evaluation of the former state of the switches, the direction of the switch current and the type of the occurring commutation.

The following computation and distribution of the turn off losses of the occurring commutation is realized in exactly the same manner as in the case of the turn on losses with the only difference that the turn off losses are distributed to the IGBTs or diodes of the other two switches.

At the end of the detection of the switching losses the new state of the switches is set. After that (or immediately after the detection of the switch current if the switch was not turned on with the new integration step) the on-state voltages of the IGBT and the diode are computed for the current values of the junction temperature and the switch current.

Finally the resulting on-state losses are distributed according to the direction of the switch current to one IGBT and one diode and the losses are added to the total losses of the active semiconductors.

Since on the one hand the switching and on-state losses are computed at each integration step and on the other hand also the fitted loss functions approximate the losses contained in the data sheet excellent, the realized loss model should describe accurately the semiconductor losses of a real matrix converter.

Furthermore the semiconductor loss model is quite fast to compute because only logical operations and some simple computations have to be carried out.

As an example, Fig. 16 shows the computed on-state voltages of the active IGBTs and diodes of the switch S_{11}. Obviously the minimum values of the on-state voltages, the bias voltages, are reached when the switch current becomes zero.

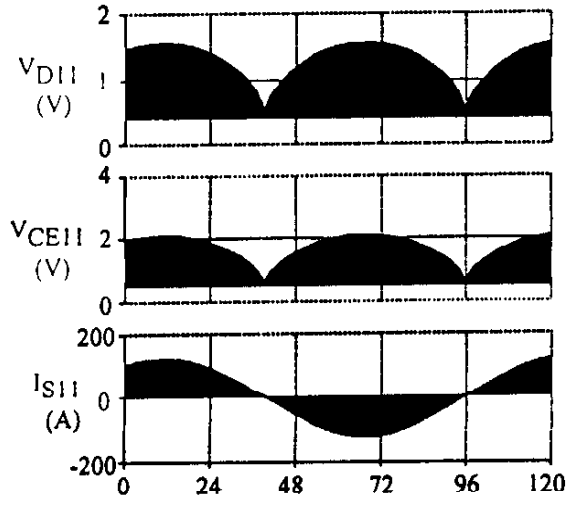

Fig. 16. On-state voltages and switch current of the switch S_{11} (SKM400GA122D; T_j=125°C; f_s=10kHz; ω=125 rpm; T=100%).

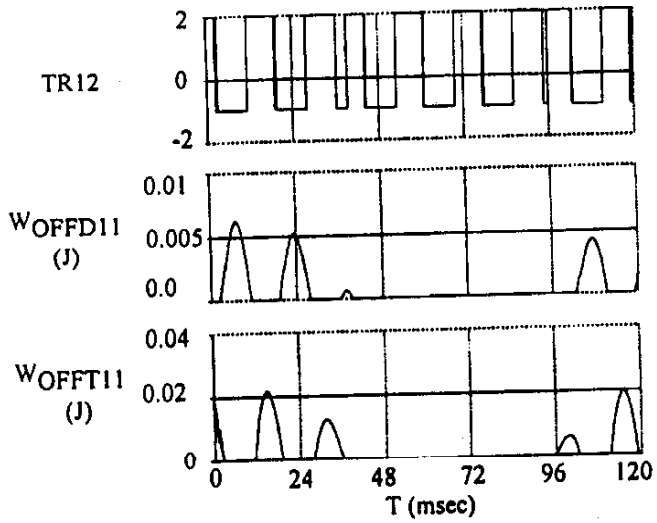

Fig. 17. Type of commutation and turn off losses of the IGBT and the diode of S_{11} which carry the positive load current (SKM400GA122D; T_j=125°C; f_s=10 kHz; ω=125 rpm; T=100%).

Fig. 17 shows the waveforms of a variable which determines the type of the commutation of the load current from S_{11} to S_{12} (TR12=2 for capacitive commutations, TR12=−1 for inductive commutations) and the turn-off losses in the diode (W_{OFFD11}) and the IGBT (W_{OFFT11}) of S_{11} which carry the positive load current. It is to be seen that the turn off losses are generated in the transistor if there is a capacitive commutation and in the diode if an inductive commutation takes place.

12. Estimated converter losses

The function of the converter losses of the rated motor torque for three different speeds in Fig. 18 shows that the losses are strongly dependent on the torque which determines the load current. The

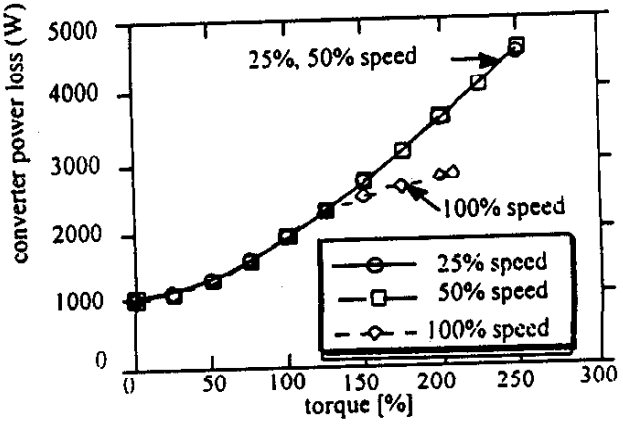

Fig. 18. Matrix converter losses versus the normalized motor torque for various speeds (SKM400GA122D; T_j=125°C; f_s=10 kHz).

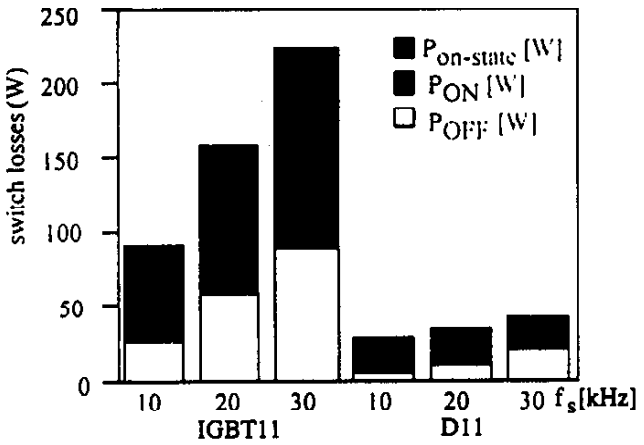

Fig. 19. Loss distribution of the IGBT and the diode of S_{11} which carry the positive load current (SKM400GA122D; T_j=125°C; f_s=10 kHz; T=100%).

decrease of the losses at high torques and high speed (e.g. 100% speed) is caused by the effective reduction of the switching frequency at the upper limit of the maximum output voltage of the converter. Fig. 19 shows the distribution of the total semiconductor losses for the IGBT and the diode of the switch S_{11} which carry the positive load current for different switching frequencies. The turn on-, turn off- and on-state losses of the IGBT at 10 kHz are approximately the same for 100% rated torque. However at high switching frequencies substantial switching losses arise which limit the converter efficiency essentially.

13. Conclusions

The implementation of the entire matrix converter/induction motor drive system into a simulation program was presented in this paper, which includes a three phase ac to ac matrix converter, an induction motor, a field oriented controller and a filter and a power source. In addition to the implementation of the drive system, a precise loss calculation model for power converters has been developed and applied to the drive system and the loss characteristics of the matrix converter were investigated. The harmonic analysis was shown to be a useful tool to develop a switching sequence combination which minimizes the harmonic contents of the matrix converter input current.

References

[1] L. Gyugyi, B.R. Pelly, Static Power Frequency Changers, Wiley, New York, 1976.
[2] A. Alesina, M. Venturini, Solid state power conversion: A Fourier analysis approach to generalized transformer synthesis, IEEE Transactions on Circuit Systems, vol. CAS-28, No. 4, 1981, pp. 319–330.
[3] ACSL Reference Manual, Mitchell and Gauthier Associates, Concord, MA, 1986.

[4] A. Alesina, M. Venturini, Analysis and design of optimum-amplitude nine-switch direct ac-ac converters, IEEE Trans. on Power Electronics, vol. 4, No. 1, Jan. 1989, pp. 101–112.
[5] D.W. Novotny, T.A. Lipo,Vector Control and Dynamics of AC Drives, Oxford Press, 1996.
[6] S. Bernet, T. Matsuo, T.A. Lipo, A Matrix Converter Using Reverse Blocking NPT-IGBTs and Optimized Pulse Patterns, Conference Record IEEE-PESC. Baveno, Italy, June 24–27, 1996, in progress.
[7] S. Bernet, Power Semiconductors as ZCS in Soft Switching Power Converters, Ph.D. thesis, TU Ilmenau (Germany), 1995.

Aims: The aim of the Journal is to provide an international forum for the dissemination of up-to-date information in the fields of Mathematics and Computers, in particular (but not exclusively) as they apply to the dynamics of systems, their Simulation and scientific computation in general. Published material ranges from short, concise research papers to more general tutorial articles.
MATHEMATICS AND COMPUTERS IN SIMULATION, published monthly, is the official organ of the International Association for Mathematics and Computers in Simulation (formerly AICA). This Association, founded in 1956, is a member of FIACC (the Five International Associations Co-ordinating Committee), together with IFIP, IFAC, IFORS and IMEKO.
Scope: Topics covered by the journal include mathematical tools (a) in the foundations of systems modelling, (b) in specific applications in science and engineering, and (c) in numerical analysis and the development of algorithms for simulation. They also include considerations (d) about computer hardware for simulation (digital, analog and hybrid) and (e) about special software and compilers. Finally, the journal publishes articles concerned (f) with the general philosophy of systems simulation, and its impact on disciplinary and interdisciplinary research. The journal also includes a Book Review section. Articles, reports and books from the international press in the disciplinary area of Mathematics and Computers in Simulation are reported.

Instructions to Authors

General

Contributions should be written in English. Manuscripts should be sent in triplicate to the Editor-in-Chief or to one of the Senior Editors. All material received will be reviewed as rapidly as possible. Authors may alternatively choose to send their manuscript in duplicate to one of the members of the Editorial Board, and one copy of their manuscript with copy of their cover letter to the Editor-in-Chief. The process of review will, in those cases, be under the responsibility of the chosen member of the Editorial Board who will forward his decision to publish/not publish to the Editor-in-Chief.

No page charge is made. Fifty reprints of each contribution are available free of charge. Additional reprints can be ordered. Please make sure that the paper is submitted in its final form. Corrections in the proof stage, other than printer's errors, should be avoided; costs arising from such corrections will be charged to the authors.

Upon acceptance of an article, the author(s) will be asked to transfer copyright of the article to the Publisher. This transfer will ensure the widest possible dissemination of information. Manuscripts should be prepared for publication in accordance with the instructions given below.

The manuscript should be typed on one side of the paper in double spacing (abstract, footnotes and references included) with wide margins. A duplicate copy should be retained by the author.
Footnotes should be avoided if possible and as brief as possible, they should be numbered consecutively.

An abstract of 10 to 20 typed lines written by the author in English as well as three to five relevant keywords will precede and introduce each article.

Special care should be given to the preparation of the drawings for figures and diagrams. Except for a reduction in size, they will appear in final printing form in exactly the same format as submitted by the author, normally they will not be redrawn by the printer. In order to make a photographic reproduction possible, all drawings should be on separate sheets, with wide margins, drawn large size, and of good quality. Exceptions are diagrams only containing formulae and a small number of straight lines (or arrows); these can be typeset:

References should be listed alphabetically, as in the following examples: books [1], articles in journals [2], papers in a contributed volume [3,4], unpublished papers [5].

[1] E. Borger, Computability, Complexity, Logic (North-Holland, Amsterdam, 1989)
[2] D. E. Knuth, Theory and Practice, Theoret. Comput. Sci. 90 (1991) 1–15.
[3] A. K. Lenstra and H. W. Lenstra, Jr., Algorithms in number theory, in: J. van Leeuwen, ed., Handbook of computer Science, Vol. A (Elsevier, Amsterdam, 1990) 673–715.
[4] M. Li, Lower bounds by Kolmogorov complexity, in: Proc. ICALP'85, Lecture Notes in Computer Science, Vol. 194 (Springer, Berlin, 1985) 383–393.
[5] A. Rajasekar, Semantics for logic programs, Ph.D. Thesis, Department of Computer Science, University of Maryland, 1989.

Electronic Submissions

The Publisher and its typesetter would be pleased to use the author's source file. If the file is suitable, proofs will be produced without rekeying the text. The Publisher reserves the right to decide whether to use the author's file or not. Typesetters have been instructed to rekey the printed copy if they suspect that the content of the file differs from the accepted paper version.

The format of the files depends on the word-processor used. Texts made with LaTeX, can be readily processed. In all other cases the preferred text format is ASCII. For LaTeX, the article should be encoded in ESP-LaTeX, standard LaTeX, or AMS-LaTeX (in document style "article"). The Elsevier-LaTeX package, together with instructions on how to prepare a file, is available from ftp://ftp.elsevier.nl/pub/styles

Authors are advised to enclose a diskette with the final revised paper version they send to their editor. Please label the disk with your name, title of the article, name of the journal and the word processor you have used. Illustrative material (original figures or high-quality glossy prints, or photographs showing a sharp contrast) should be included separately on paper. Upon receipt by the publisher, missing disks will be requested by the publisher's Log-In department. Please make sure the version your submit by email then, is exactly the same as the version accepted by the editor.

Electronic submission: Non-LaTex

Only the final accepted manuscript can be submitted on disk, along with a paper-printed version which is identical to the file. Please label the disk with your name, and mention which word processor you have used.

The word-processed text should be in single column format. Keep the layout of the text as simple as possible; in particular, do not use the word-processor's options to justify the text or to hyphenate the words.

The electronic text should be prepared in a way very similar to that of conventional manuscripts (see also Guide for Authors). The list of references, tables and figure legends should be compiled separately from the main text. Do not reserve space for the figures and tables in the text; instead, indicate their approximate locations, either directly in the electronic text or on the manuscript.

The final text should be submitted **both in manuscript form and on diskette.** Use standard 3.5" or 5.25" diskettes for this purpose. Both double density (DD) and high density (HD) diskettes are acceptable.

It is recommended to store the main text, list of references, tables and figure legends in separate text files with clearly identifiable file names (for example, with extensions .TXT, .REF, .TBL, .FIG).

The format of the files depends on the word-processor used. Texts made with DEC WPS PLUS, Display Write, First Choice, IBM Writing Assistant, Microsoft Word, Multimate, PFS: Write, Professional Writer, Samma Word, Sprint, Total Word, Volkswriter, Wang PC, WordMARC, WordPerfect, Wordstar, or files supplied in DCA.RFT format can be readily processed. In all other cases the preferred text format is ASCII.

Essential is that name and version of the word-processing program and the type of computer on which the text was prepared is clearly indicated on the diskette label or the accompanying checklist.

The manuscript may contain parts (e.g. formulas or complex tables) or last-minute corrections which are not included in the text on diskette; however, if this is the case then the differences with the diskette version should be clearly marked on the manuscript.

Illustrative material (original figures or high-quality glossy prints, or photographs showing a sharp contrast) should be included separately.